NJIT CAMS Technical Report:

Subthreshold amplitude and phase resonance in single cells *

Horacio G. Rotstein[1]
[1] Department of Mathematical Sciences
New Jersey Institute of Technology
Newark, NJ 07102, USA

October 22, 2013

Synonyms

Membrane potential resonance, membrane potential or subthreshold preferred frequency responses to oscillatory inputs.

Definition

Subthreshold (or membrane potential) resonance refers to the ability of neurons to exhibit a peak in their voltage amplitude response to oscillatory input currents at a preferred (resonant) frequency.

Subthreshold (or membrane potential) phase-resonance refers to the ability of neurons to exhibit a zero-phase (or zero-phase-shift) response to oscillatory inputs currents at a non-zero (phase-resonant) frequency.

Linear subthreshold resonance refers to the subthreshold resonant properties (amplitude and phase) in linear models. In this article we focus on 2D and 3D linear and linearized conductance-based models.

*To be published in the Encyclopedia of computational neuroscience

Detailed Description

Introduction

Subthreshold resonance has been observed in various neuron types in the hippocampus and the entorhinal cortex (Hutcheon and Yarom 2000; Pike et al. 2000; Schreiber et al. 2004; Zemankovics et al. 2010; Hu et al. 2002, 2009; Leung and Yu 1998; Erchova et al. 2004; Heys et al. 2010; Engel et al. 2008; Wang et al. 2006) as well as in other neural systems (Hutcheon et al. 1996b, 1994; Art et al. 1986; Tohidi and Nadim 2009; Tseng and Nadim 2010; Castro-Alamancos et al. 2007; Wu et al. 2001; Gastrein et al. 2011; Sciamanna and J. 2011). The functionality of the resonant properties of neurons has not been established yet. However, since the resonant frequency of principal cells in the entorhinal cortex and the hippocampus lies in the theta frequency range, resonance has been implicated in the generation of rhythmic activity at theta and nested theta/gamma frequencies.

Theoretical studies on resonance have been performed using linear models (either caricature models or linearizations of conductance-based models) or by direct simulation conductance-based models (Richardson et al. 2003; Gutfreund et al. 1995; Schreiber et al. 2004; Haas and White 2002; Alexander et al. 1990; Izhikevich 2001, 2002; Hutcheon et al. 1996a, 1994; Reinker et al. 2004; Rotstein and Nadim 2013; Rotstein 2013)

Conductance-based models

In this article we discuss the subthreshold resonant properties of neurons in the context of biophysical (conductance-based) models (Skinner 2006; Hodgkin and Huxley 1952) whose subthershold dynamics are governed by the following equations

$$C\,\frac{dV}{dt} = -I_L - \sum_k I_k + I_{app} + I_{in}(t), \tag{1}$$

$$\frac{dx_k}{dt} = \frac{x_{k,\infty}(V) - x_k}{\tau_{k,x}(V)}, \qquad k = 1, 2. \tag{2}$$

In the current-balance equation (1), V is the membrane potential (mV), t is time (msec), C is the membrane capacitance (μF/cm^2), I_{app} is the applied bias (DC) current (μA/cm^2), $I_L = G_L\,(V - E_L)$ is the leak current, and $I_k = G_k\,x_k\,(V - E_k)$ are generic expressions for ionic currents (with k an index) with maximal conductance G_k (mS/cm^2) and reversal potentials E_k (mV) respectively. The dynamics of the gating variables x_k are governed by the kinetic equations (2) where $x_{k,\infty}(V)$ and $\tau_{k,x}(V)$ are the voltage-dependent activation/inactivation curves and time constants respectively. The generic ionic currents I_k we consider here are restricted to have a single gating variable x_k and to be linear in x_k. The persistent sodium, h- (hyperpolarization-activated, mixed-cation, inward), and slow-potassium (M-type) currents found to be responsible for the generation of subthreshold resonance in neurons of the hippocampus and the entorhinal cortex have this form (Schreiber et al. 2004; Hu et al. 2002, 2009; Pike et al. 2000; Rotstein et al. 2006; Izhikevich 2006). Our discussion of subthreshold resonance can be easily adapted to ionic currents having two gating variables raised to powers not necessarily equal to one such as calcium currents (Hutcheon and Yarom 2000).

The function $I_{in}(t)$ in eq. (1) is an oscillatory input current (μA/cm^2) of the form

$$I_{in}(t) = A_{in}\, sin(\Omega\, t) \qquad \text{with} \qquad \Omega = \frac{2\pi f}{1000}, \tag{3}$$

where f is the input frequency (Hz).

We focus on two- and three-dimensional models describing the dynamics of V and either one (2D) or two (3D) gating variables. Additional currents whose gating variables evolve on a very fast time scale (as compared to the other variables) can be included by using the adiabatic approximation $x_k = x_{k,\infty}(V)$. Here we include one such fast current ($I_3 = G_3\, x_{3,\infty}(V)\,(V - E_3)$). Additional fast currents can be included without significantly changing the formalism used here.

Linearized conductance-based models

Linearization of the autonomous part ($I_{in}(t) = 0$) of system (1)-(2) around the fixed-point $(\bar{V}, \bar{x}_1, \bar{x}_2)$ yields (Richardson et al. 2003)

$$C\,\frac{dv}{dt} = -g_L v - g_1 w_1 - g_2\, w_2 + I_{in}(t), \tag{4}$$

$$\bar{\tau}_1 \frac{dw_1}{dt} = v - w_1, \tag{5}$$

$$\bar{\tau}_2 \frac{dw_2}{dt} = v - w_2, \tag{6}$$

where

$$v = V - \bar{V}, \qquad w_1 = \frac{x_1 - \bar{x}_1}{x'_{1,\infty}(\bar{V})}, \qquad w_2 = \frac{x_2 - \bar{x}_2}{x'_{2,\infty}(\bar{V})}, \tag{7}$$

$$\bar{x}_k = x_{k,\infty}(\bar{V}), \qquad \bar{\tau}_k = \tau_{x,k}(\bar{V}) \qquad k = 1, 2, \tag{8}$$

$$g_k = G_k\, x'_{k,\infty}(\bar{V})\,(\bar{V} - E_k), \qquad k = 1, 2, 3, \tag{9}$$

and

$$g_L = G_L + G_1\, x_{1,\infty}(\bar{V}) + G_2\, x_{2,\infty}(\bar{V}) + G_3\, x_{3,\infty}(\bar{V}) + g_3. \tag{10}$$

In (7) and (9) $x'_{k,\infty} = dx_k/dV$ ($k = 1, 2, 3$). Note that the gating variables w_1 and w_2 in (7) have units of voltage ($[v] = [w_1] =$V).

The effective leak conductance g_L (10) contains information about the biophysical leak conductance G_L, the ionic conductances, and their associated voltage-dependent activation/inactivation curves. The fast ionic current I_3 contributes to g_L with an additional term (g_3). The signs of the effective ionic conductances g_k determine whether the associated gating variables are either resonant ($g_k > 0$) or amplifying ($g_k < 0$) (Richardson et al. 2003; Hutcheon and Yarom 2000). All terms in g_L are positive except for the last one that can be either positive or negative. Specifically, g_L can become negative for negative enough values of g_3.

System (4)-(6) can be rescaled by defining the following dimensionless time and parameters

$$\hat{t} = \frac{t}{\bar{\tau}_1}, \qquad \gamma_L = \frac{g_L \bar{\tau}_1}{C}, \qquad \gamma_1 = \frac{g_1 \bar{\tau}_1}{C}, \qquad \gamma_2 = \frac{g_2 \bar{\tau}_1}{C}, \qquad \eta = \frac{\bar{\tau}_1}{\bar{\tau}_2}. \tag{11}$$

Substitution of (11) into (4)-(6) and a further rearrangment of terms yields

$$\frac{dv}{d\hat{t}} = -\gamma_L v - \gamma_1 w_1 - \gamma_2 w_2 + \hat{I}_{in}(t), \tag{12}$$

$$\frac{dw_1}{d\hat{t}} = v - w_1, \tag{13}$$

$$\frac{dw_2}{d\hat{t}} = \eta\,[v - w_2], \tag{14}$$

where γ_L, γ_1 and γ_2 are the dimensionless effective conductances and

$$\hat{I}_{in}(t) = \hat{A}_{in}\, sin(2\pi f\, \bar{\tau}_1\, \hat{t}/1000) \qquad \text{with} \quad \hat{A}_{in} = \frac{A_{in}\bar{\tau}_1}{C}. \tag{15}$$

Voltage response, impedance, impedance amplitude and phase

The voltage response of a neuron receiving an oscillatory input current is typically measured in terms of the so-called impedance function $Z(f)$ defined as the quotient between the Fourier transforms of the output voltage $V_{out}(t)$ and the input current $I_{in}(t)$

$$Z(f) = \frac{\mathcal{F}[V_{out}(t)](f)}{\mathcal{F}[I_{in}(t)](f)}. \tag{16}$$

The impedance $Z(f)$ is a complex quantity with amplitude $|Z(f)|$ and phase $\Phi(f)$. For simplicity we refer to the impedance amplitude $|Z(f)|$ simply as the impedance $Z(f)$.

For a linear system receiving sinusoidal input currents of the form (3), the voltage response is given by

$$V_{out}(t; f) = A_{out}(f)\, \sin\left(\Omega\, t + \Phi(f)\right) \tag{17}$$

where $A_{out}(f)$ is the amplitude and the phase $\Phi(f)$ (or phase-shift) is the difference between the peaks of the input current $I_{in}(t; f)$ and the output voltage $V_{out}(t; f)$. The impedance amplitude is given by

$$|\, Z(f)\,| = \frac{A_{out}(f)}{A_{in}}. \tag{18}$$

For linear systems (18) is equivalent to (16).

Several authors have used the so called ZAP current (Puil et al. 1986)

$$I_{in}(t) = I_{Zap}(t) = A_{in}\, \sin(2\,\pi\, f(t)\, t), \qquad f(t) = \frac{f_M\, t}{2\, T_M}, \tag{19}$$

that sweeps through a given range of frequencies over time with a maximum frequency f_M and a stimulus length T_M. (Other types of time-dependent input frequencies have also been used (Tseng and Nadim 2010).) The corresponding impedance function can be computed using (16).

Impedance and phase profiles for 2D and 3D linear systems: Analytic expressions

Analytic expressions for the impedance and phase profiles for linear systems can be computed analytically. We use the following generic system

$$\begin{cases} X' = a\,X + b\,Y + c\,Z + A_{in}\,e^{i\,\Omega\,t}, \\ Y' = \alpha\,X + p\,Y, \\ Z' = \beta\,X + q\,Z, \end{cases} \tag{20}$$

where a, b, c, α, β, p and q are constant, $\Omega > 0$ and $A_{in} \geq 0$.

The characteristic polynomial for the corresponding homogeneous system ($A_{in} = 0$) is given by

$$r^3 - (a + p + q)\,r^2 + (a\,p + a\,q + p\,q - c\,\beta - b\,\alpha)\,r + b\,\alpha\,q + c\,\beta\,p - a\,p\,q = 0. \tag{21}$$

The particular solution to system (20) has the form

$$X_p(t) = A_{out}\,e^{i\,\Omega\,t}, \qquad Y_p(t) = B_{out}\,e^{i\,\Omega\,t} \qquad \text{and} \qquad Z_p(t) = C_{out}\,e^{i\,\Omega\,t}, \tag{22}$$

Substituting (22) into system (20), rearranging terms, and solving the resulting algebraic system one obtains

$$Z(\Omega) = \frac{A_{out}}{A_{in}} = \frac{P_r(\Omega) + i\,P_i(\Omega)}{Q_r(\Omega) + i\,Q_i(\Omega)} \tag{23}$$

where

$$P_r(\Omega) = p\,q - \Omega^2, \tag{24}$$

$$P_i(\Omega) = -(p + q)\,\Omega, \tag{25}$$

$$Q_r(\Omega) = (a + p + q)\,\Omega^2 - a\,p\,q + b\,\alpha\,q + c\,\beta\,p, \tag{26}$$

and

$$Q_i(\Omega) = (a\,p + a\,q + p\,q - b\,\alpha - c\,\beta - \Omega^2)\,\Omega. \tag{27}$$

From (23)

$$|Z|^2(\Omega) := \frac{A_{out}^2}{A_{in}^2} = \frac{P_r^2(\Omega) + P_i^2(\Omega)}{Q_r^2(\Omega) + Q_i^2(\Omega)} \tag{28}$$

and

$$\Phi = \tan^{-1}\frac{P_r(\Omega)\,Q_i(\Omega) - P_i(\Omega)\,Q_r(\Omega)}{P_r(\Omega)\,Q_r(\Omega) + P_i(\Omega)\,Q_i(\Omega)}. \tag{29}$$

For a 2D linear system ($c = q = 0$), the characteristic polynomial for the corresponding homogeneous system ($A_{in} = 0$) is given by

$$r^2 - (a+p)\,r + (a\,p - b\,\alpha) \;= 0. \tag{30}$$

The roots of the characteristic polynomial are given by

$$r_{1,2} = \frac{(a+p) \pm \sqrt{(a-p)^2 + 4\,b\,\alpha}}{2}. \tag{31}$$

From eq. (31), the homogeneous (unforced) system displays oscillatory solutions with a natural frequency f_{nat} (Hz) given by

$$f_{nat} = \mu\,\frac{1000}{2\,\pi}, \qquad\qquad \mu = \sqrt{-4b\alpha - (a-p)^2}, \tag{32}$$

provided $4\,b\,\alpha + (a-p)^2 < 0$.

The impedance amplitude and phase are given, respectively, by

$$|Z(\Omega)|^2 := \frac{A_{out}^2}{A_{in}^2} = \frac{p^2 + \Omega^2}{[\,a\,p - b\,\alpha - \Omega^2\,]^2 + (a+p)^2\,\Omega^2}, \tag{33}$$

and

$$\Phi(\Omega) = \tan^{-1}\frac{(a\,p - b\,\alpha - \Omega^2)\;\Omega - (a+p)\,\Omega\,p}{(a\,p - b\,\alpha - \Omega^2)\,p + (a+p)\;\Omega^2}. \tag{34}$$

Impedance and phase profiles for 2D and 3D linear systems: resonance and phase-resonance

The impedance and phase profiles are the curves of the impedance amplitude (Z) and phase (Φ) as a function of the input frequency f respectively.

For 2D linear systems the impedance profile is either a decreasing function of f (red curve in Fig. 1-A1) representing a low-pass filter response, or it exhibits a peak at a non-zero input frequency (blue curve in Fig. 1-A1) representing a resonant response at the resonant frequency f_{res} (impedance peak). The phase profile is either an increasing function of f converging asymptotically to $\Phi = \pi/2$ (red curve in Fig. 1-A2) representing a delayed response for all values of f, or it exhibits a zero-phase response at a non-zero input frequency (blue curve in Fig. 1-A2) called the phase-resonant frequency f_{phas}. For input frequencies $f = f_{phas}$ the input current and output voltage peak at the same time. For input frequencies $f < f_{phas}$, the voltage response is advanced, while for input frequencies $f > f_{phas}$ the voltage response is delayed.

The voltage response for 3D linear systems is more complex than for 2D linear systems. The impedance profile may exhibit a local minimum at an input frequency f_{min} in addition to the peak at the resonant frequency (Fig. 1-B1). The phase profile may have an additional zero-frequency cross (Fig. 1-B1). For input frequencies $f = f_{phas,m}$ and $f = f_{phas,M}$ the input current and output voltage peak at the same time. The voltage response is delayed for input frequencies $f < f_{phas,m}$ and $f > f_{phas,M}$ and advanced for input frequencies f such that $f_{phas,m} < f < f_{phas,M}$.

Attributes of the Impedance and phase profiles for 2D and 3D linear systems

For mechanistic purposes one wishes to track the changes in the impedance and phase profiles as a chosen model parameter changes. To this end it is useful to characterize these graphs using a small number of attributes rather than the information corresponding to the whole curves.

For 2D linear systems the impedance profile can be characterized by four attributes (Fig. 1-A1): the resonant frequency f_{res}, the maximum impedance Z_{max}, the resonance amplitude $Q_Z = Z_{max} - Z(0)$, and the half-bandwidth $\Lambda_{1/2}$. Some authors define the resonance amplitude as $Q = Z_{max}/Z(0)$. For a low-pass filter response $Q_Z = 0$ ($Q = 1$). Resonance requires $Q_Z > 0$ ($Q > 1$). The phase profile can be charaterized by two attributes (Fig. 1-A2): the phase-resonant frequency f_{phas} and the minimum phase Φ_{min}. A phase-resonant response requires $\Phi_{min} < 0$.

For 3D linear systems the impedance profile can be characterized by f_{res}, Z_{max}, Q_Z, $\Lambda_{1/2}$, and two additional attributes (Fig. 1-B1): the minimum phase Z_{min} and the minimum frequency f_{min}. The phase profile can be characterized by f_{phas} (or $f_{phas,M}$), Φ_{min}, and two additional attributes (Fig. 1-B2): the maximum phase Φ_{max}, and the minimum zero-crossing frequency $f_{phas,m}$. The maximum zero-crossing frequency is $f_{phas,M}$ is equal to f_{phas} in 2D linear systems.

Resonant and amplifying currents and gating variables

Subthreshold resonance results from a combination of low- and high-pass filter mechanisms that have been described in terms of ionic currents (Hutcheon and Yarom 2000). Passive currents (in particular capacitive currents) act as low-pass filters (see Fig. 1-A1, red curve).

The so-called resonant currents create a preferred frequency band by slowly opposing voltage changes. Amplifying currents, on the other hand, have been argued to generate a positive feedback effect that amplifies voltage changes, and hence make existing resonances more pronounced (Hutcheon and Yarom 2000) but they do not create resonance by themselves. Prototypical examples of resonant currents are (inward) hyperpolarization-activated h-currents (I_h) (Haas and White 2002; Schreiber et al. 2004; Hutcheon et al. 1996b) and (outward) slow potassium currents (I_{Ks} or I_M) (Gutfreund et al. 1995). Prototypical examples of amplifying currents are persistent sodium currents (I_p) (Haas and White 2002; Schreiber et al. 2004; Hutcheon et al. 1996b; Gutfreund et al. 1995) and high-threshold calcium currents (I_L) (Hutcheon and Yarom 2000). The low-threshold calcium current I_T is both resonant and amplifying (Hutcheon and Yarom 2000).

In fact, the resonant and amplifying abilities do not reside in the currents themselves but in their gating variables (Hutcheon and Yarom 2000; Richardson et al. 2003). Inward inactivating and outward activating gating variables produce resonant effects . Inward activating and outward inactivating gating variables produce amplifying effects.

The resonant or amplifying nature of a gating variable can be predicted from the definition of the effective ionic conductances g_k in (9), which are positive for resonant gating variables and negative for amplifying gating variables (Richardson et al. 2003).

In addition to generating resonance and amplifying existing resonances, changes in the resonant and amplifying conductances affect other attributes of the impedance and phase profiles (Rotstein and Nadim 2013).

Subthreshold resonance, phase-resonance and intrinsic oscillations

Subthreshold resonance, phase-resonance and intrinsic (damped) oscillations are different phenomena generated by related, but different mechanisms (Richardson et al. 2003; Rotstein and Nadim 2013; Rotstein 2013). This is illustrated in Fig. 2 for the 2D linear system (12)-(13) ($\gamma_2 = 0$).

The differences between these phenomena are clearly illustrated by the so-called λ - ω systems (Kopell and Howard 1973)

$$\frac{dx}{dt} = -\lambda\, x - \omega\, y, \tag{35}$$

$$\frac{dy}{dt} = \omega\, x - \lambda\, y, \tag{36}$$

with $\lambda > 0$ and $\omega > 0$.

The eigenvalues and natural frequency are given by

$$r_{1,2} = -\lambda \pm \sqrt{-\omega^2} \qquad \text{and} \qquad \Omega_{nat} = \omega. \tag{37}$$

The resonant and phase-resonant frequencies are given by

$$\Omega_{res} = \sqrt{-\lambda^2 + \omega\,\sqrt{4\,\lambda^2 + \omega^2}} \qquad \text{and} \qquad \Omega_{phas} = \sqrt{\omega^2 - \lambda^2}. \tag{38}$$

For $\lambda = 0$ (no damping) $\Omega_{nat} = \Omega_{res} = \Omega_{phas}$, while for other values of λ these three quantities are different.

System (35)-(36) can be transformed into a rescaled system of the form (12)-(13) (with $\gamma_2 = 0$) by defining

$$v = \omega\, x, \qquad w = \lambda\, y, \qquad \hat{t} = \lambda\, t, \tag{39}$$

and

$$\gamma_L = 1 \qquad \gamma_1 = \frac{\omega^2}{\lambda^2}. \tag{40}$$

More generally, the differences among the subthreshold resonance, phase-resonance and natural frequencies are illustrated by the 2D linear system (4)-(5) ($g_2 = 0$) where

$$\Omega_{nat} = \frac{1}{2\,\tau_1\, C}\,\sqrt{4\, g_1\, \tau_1\, C + (C - g_L\, \tau_1)^2}, \tag{41}$$

$$\Omega_{res} = \frac{1}{\tau_1}\,\sqrt{\sqrt{\frac{g_1^2\,\tau_1^2 + 2\, g_L\, g_1\, \tau_1^2 + 2\, g_1\, \tau_1\, C}{C^2}} - 1}, \tag{42}$$

and

$$\Omega_{phas} = \frac{1}{\tau_1}\,\sqrt{\frac{g_1\,\tau_1 - C}{C}}. \tag{43}$$

Mechanisms of generation of subthreshold resonance and phase-resonance

The investigation of the mechanisms of generation of resonance and phase-resonance consists of tracking the changes in the impedance and phase profiles that result from changes in certain model parameters of interest while keeping the remaining parameters fixed. This task is greatly simplified if one uses the attributes of the impedance and phase profiles instead of the full graphs.

This mechanistic investigation can be performed at different modeling levels by looking at (i) the dimensionless effective parameters in the rescaled system (12)-(14), (ii) the effective parameters in the linearized system (4)-(6), or (iii) the biophysical parameters in the original conductance-based model.

For the 2D rescaled system ($\gamma_2 = 0$) heat graphs of the attributes of the impedance and phase profiles can be plotted in the γ_L-γ_1 parameter space presented in Fig. 2 (Rotstein and Nadim 2013). These attribute graphs can be used to investigate the effects of changes in parameters at the different levels of description mentioned above including (i) the effects of changes in the dimensionless effective conductances γ_L and γ_1, by moving in either horizontal (γ_L) and vertical (γ_1) directions respectively, (ii) the effects of changes in the effective conductances g_L and g_1, by moving in either horizontal (g_L) and vertical directions (g_1) using the rescaling (11) to account for the values of τ_1 and C, (iii) the effects of changes in the time constant τ_1, by moving along oblique lines (parametrized by τ_1) with slope g_1/g_L in the attribute graphs, and (iv) the effects of changes in the biophysical parameters of the original conductance-based model to the linear level of approximation, by using the formulas (9) and (10) for the effective ionic (g_k) and leak (g_L) conductances in terms of the biophysical conductances (G_L and G_k), resting potential, and other biophysical parameters. Changes in the biophysical conductances generate nonlinear curves in the γ_L-γ_1 parameter space (Rotstein and Nadim 2013). These nonlinear curves reflect the different effects caused by different types of resonant and amplifying currents (Rotstein and Nadim 2013).

This approach can be extented to 3D systems by looking at appropriate projections. Alternatively, one can investigate the linearized system (4)-(6) directly. For the rescaled system (12)-(14) one varies the dimensionless effective conductances γ_L, γ_1 and γ_2 and the time scale parameter η.

Acknowledgments

The author wishes to thank Farzan Nadim and Frances Skinner for useful comments. This work was supported by NSF grant DMS-1313861 (HGR).

References

Alexander JC, Doedel EJ, and Othmer HG, On the resonance structure in a forced excitable system. *SIAM J Appl Math* 50: 1373–1418, 1990.

Art JJ, Crawford AC, and Fettiplace R, Electrical resonance and membrane currents in turtle cochlear hair cells. *Hear Res* 22: 31–36, 1986.

Castro-Alamancos MA, Rigas P, and Tawara-Hirata Y, Resonance (approximately 10 hz) of

excitatory networks in motor cortex: Effects of voltage-dependent ion channel blockers. *J Physiol* 578: 173–191, 2007.

Engel TA, Schimansky-Geier L, Herz AV, Schreiber S, and Erchova I, Subthreshold membrane-potential resonances shape spike-train patterns in the entorhinal cortex. *J Neurophysiol* 100: 1576–1588, 2008.

Erchova I, Kreck G, Heinemann U, and Herz AVM, Dynamics of rat entorhinal cortex layer II and III cells: Characteristics of membrane potential resonance at rest predict oscillation properties near threshold. *J Physiol* 560: 89–110, 2004.

Gastrein P, Campanac E, Gasselin C, Cudmore RH, Bialowas A, Carlier E, Fronzaroli-Molinieres L, Ankri N, and Debanne D, The role of hyperpolarization-activated cationic current in spike-time precision and intrinsic resonance in cortical neurons *in vitro*. *J Physiol* 589: 3753–3773, 2011.

Gutfreund Y, Yarom Y, and Segev I, Subthreshold oscillations and resonant frequency in guinea pig cortical neurons: Physiology and modeling. *J Physiol* 483: 621–640, 1995.

Haas JS and White JA, Frequency selectivity of layer II stellate cells in the medial entorhinal cortex. *J Neurophysiol* 88: 2422–2429, 2002.

Heys JG, Giacomo LM, and Hasselmo ME, Cholinergic modulation of the resonance properties of stellate cells in layer II of the medial entorhinal. *J Neurophysiol* 104: 258–270, 2010.

Hodgkin AL and Huxley AF, A quantitative description of membrane current and its application to conductance and excitation in nerve. *J Physiol* 117: 500–544, 1952.

Hu H, Vervaeke K, and Graham JF L J Storm, Complementary theta resonance filtering by two spatially segregated mechanisms in CA1 hippocampal pyramidal neurons. *J Neurosci* 29: 14472–14483, 2009.

Hu H, Vervaeke K, and Storm JF, Two forms of electrical resonance at theta frequencies generated by M-current, h-current and persistent Na^+ current in rat hippocampal pyramidal cells. *J Physiol* 545.3: 783–805, 2002.

Hutcheon B, Miura RM, and Puil E, Models of subthreshold membrane resonance in neocortical neurons. *J Neurophysiol* 76: 698–714, 1996a.

Hutcheon B, Miura RM, and Puil E, Subthreshold membrane resonance in neocortical neurons. *J Neurophysiol* 76: 683–697, 1996b.

Hutcheon B, Miura RM, Yarom Y, and Puil E, Low threshold calcium current and resonance in thalamic neurons: A model of frequency preference. *J Neurophysiol* 71: 583–594, 1994.

Hutcheon B and Yarom Y, Resonance oscillations and the intrinsic frequency preferences in neurons. *Trends Neurosci* 23: 216–222, 2000.

Izhikevich E, *Dynamical Systems in Neuroscience: The geometry of excitability and bursting*. MIT Press (Cambridge, Massachusetts), 2006.

Izhikevich EM, Resonate-and-fire neurons. *Neural Networks* 14: 883–894, 2001.

Izhikevich EM, Resonance and selective communication via bursts in neurons having subthreshold oscillations. *Biosystems* 67: 95–102, 2002.

Kopell N and Howard LN, Plane wave solutions to reaction diffusion systems. *Studies in Appl Math* 42: 291–328, 1973.

Leung LS and Yu HW, Theta-frequency resonance in hippocampal CA1 neurons *in vitro* demonstrated by sinusoidal current injection. *J Neurophysiol* 79: 1592–1596, 1998.

Pike FG, Goddard RS, Suckling JM, Ganter P, Kasthuri N, and Paulsen O, Distinct frequency preferences of different types of rat hippocampal neurons in response to oscillatory input currents. *J Physiol* 529: 205–213, 2000.

Puil E, Gimbarzevsky B, and Miura RM, Quantification of membrane properties of trigeminal root ganglions in guinea pigs. *J Neurophysiol* 55: 995–1016, 1986.

Reinker S, Puil E, and Miura RM, Membrane resonance and stochastic resonance modulate firing patterns of thalamocortical neurons. *Journal of Computational Neuroscience* 16: 15–25, 2004.

Richardson MJE, Brunel N, and Hakim V, From subthreshold to firing-rate resonance. *J Neurophysiol* 89: 2538–2554, 2003.

Rotstein HG, Frequency preference response to oscillatory inputs in two-dimensional neural models: a dynamical systems approach to subthreshold amplitude and phase resonance. *Submitted* 2013.

Rotstein HG and Nadim F, Interaction between resonant and amplifying currents in two-dimensional neural models of frequency preference response to oscillatory input currents. *J Comp Neurosci (in press)* 2013.

Rotstein HG, Oppermann T, White JA, and Kopell N, A reduced model for medial entorhinal cortex stellate cells: Subthreshold oscillations, spiking and synchronization. *Journal of Computational Neuroscience* 21: 271–292, 2006.

Schreiber S, Erchova I, Heinemann U, and Herz AV, Subthreshold resonance explains the frequency-dependent integration of periodic as well as random stimuli in the entorhinal cortex. *J Neurophysiol* 92: 408–415, 2004.

Sciamanna G and J WC, The ionic mechanism of gamma resonance in rat striatal fast-spiking neurons. *J Neurophysiol* 106: 2936–2949, 2011.

Skinner FK, Conductance-based models. *Scholarpedia* 1: 1408, 2006.

Tohidi V and Nadim F, Membrane resonance in bursting pacemaker neurons of an oscillatory network is correlated with network frequency. *J Neurosci* 6427: 6435, 2009.

Tseng H and Nadim F, The membrane potential waveform on bursting pacemaker neurons is a predictor of their preferred frequency and the network cycle frequency. *J Neurosci* 30: 10809–10819, 2010.

Wang WT, Wan YH, Zhu JL, Lei GS, Wang YY, Zhang P, and Hu SJ, Theta-frequency membrane resonance and its ionic mechanisms in rat subicular pyramidal neurons. *Neuroscience* 140: 45–55, 2006.

Wu N, Hsiao CF, and Chandler SH, Membrane resonance and subthreshold membrane oscillations in mesencephalic v neurons: Participants in burst generation. *J Neurosci* 21: 3729–3739, 2001.

Zemankovics R, Káli S, Paulsen O, Freund TF, and Hájos N, Differences in subthershold resonance of hippocampal pyramidal cells and interneurons: The role of h-current and passive membrane characteristics. *J Physiol* 588: 2109–2132, 2010.

Figure Legends

Figure 1. Impedance (Z) and phase (Φ) profiles (curves of Z and Φ vs. the input frequency f) for representative 2D (A) and 3D (B) linear systems. A1: The impedance Z is characterized by four attributes: the resonant frequency f_{res}, the impedance peak Z_{max}, the resonance amplitude $Q_Z = Z_{max} - Z(0)$, and the half-bandwidth $\Lambda_{1/2}$. **A2:** The phase Φ is characterized by two attributes: the zero-crossing frequency f_{phas} and the phase minimum Φ_{min}. For this example, $f_{phas} < f_{res}$. **B1:** The impedance Z is characterized by two additional attributes: the antiresonant frequency f_{ares} and the impedance local minimum Z_{min}. **B2:** The phase Φ is characterized by two additional attributes: the phase local maximum Φ_{max} and the zero-crossing phase $f_{phas,m}$ on the descending portion of Φ. The zero-crossing phase $f_{phas,M}$ on the ascending portion of Φ is as f_{phas} in panel A1. The curves in all panels were computed using system (4)-(6) with **A1 (blue curve):** $g_L = 1$, $g_1 = 0$, $g_2 = 0$, and $\tau_1 = 10$. **A1 (red curve):** $g_L = 0$, $g_1 = 4$, $g_2 = 0$, and $\tau_1 = 1$ (red curve). **A2 (blue curve):** $g_L = 1$, $g_1 = 0$, $g_2 = 0$, and $\tau_1 = 10$. **A2 (red curve):** $g_L = 0$, $g_1 = 0.5$, $g_2 = 0$, and $\tau_1 = 1$. **B1:** $g_L = 1$, $g_1 = 0.8$, $g_2 = -0.6$, $\tau_1 = 10$ and $\tau_2 = 100$. **B2:** $g_L = 1$, $g_1 = 1$, $g_2 = -0.9$, $\tau_1 = 10$ and $\tau_2 = 100$. In all panels $C = 1$ and $A_{in} = 1$.

Figure 2. Stability and resonance diagrams for the reduced 2D linear system (12)-(13) ($\gamma_2 = 0$) in γ_L-γ_1 parameter space. **A.** Stability diagram. The blue curves separate between regions with different stability properties. **B.** Resonance diagram. The red curves separate between regions where the system does (above) and does not (below) exhibit resonance. **C.** Phase-resonance diagram. The green line separates between regions where the system does (above) and does not (below) exhibit phase-resonance. **D.** Superimposed stability (blue curves), resonance (red curves) and phase-resonance (green line) diagrams showing that intrinsic oscillations and resonance may occur in the absence of the other and resonance may occur in the absence of phase-resonance. The right panel is a magnification of the left one.

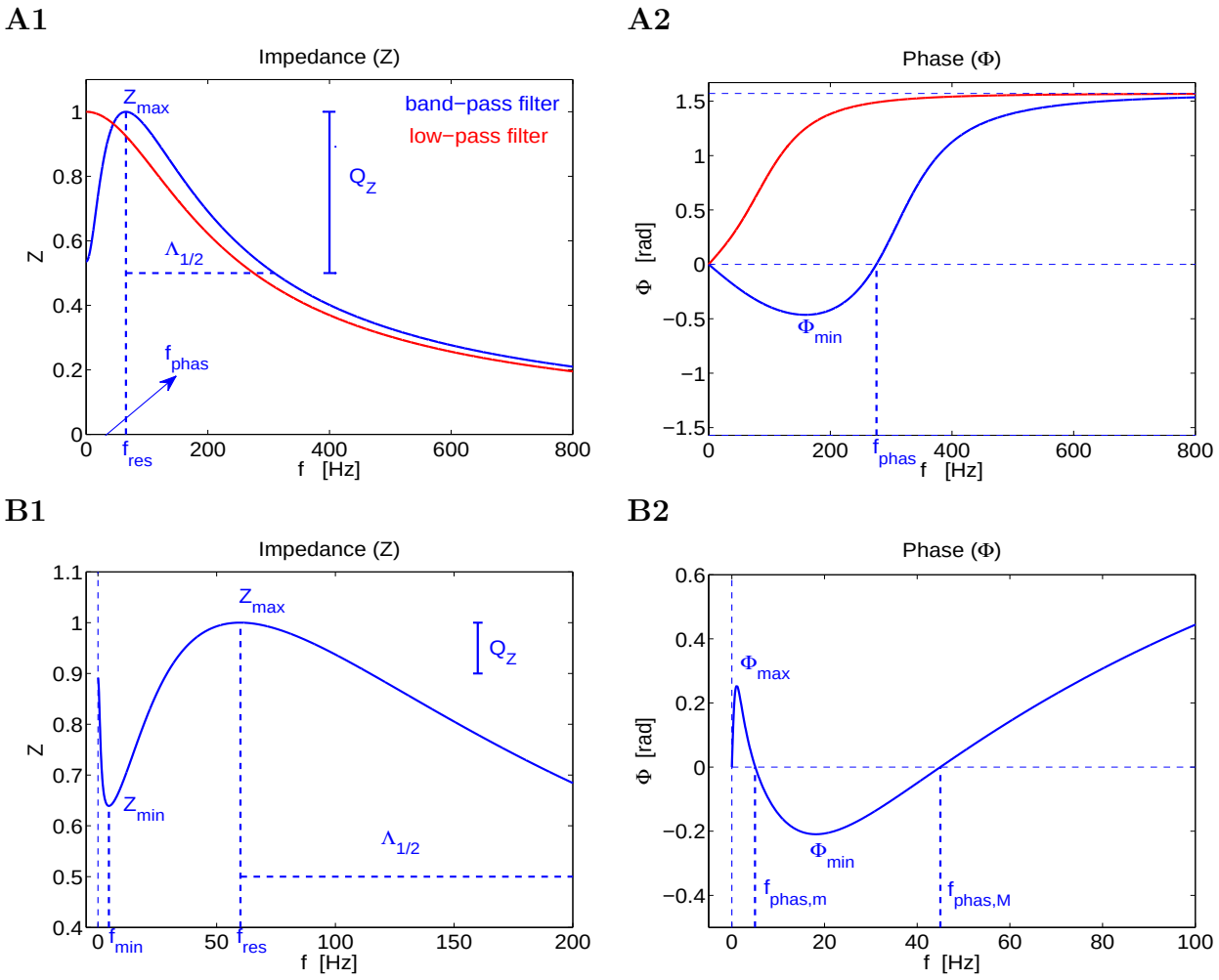

Figure 1: **Impedance (Z) and phase (Φ) profiles (curves of Z and Φ vs. the input frequency f) for representative 2D (A) and 3D (B) linear systems.**

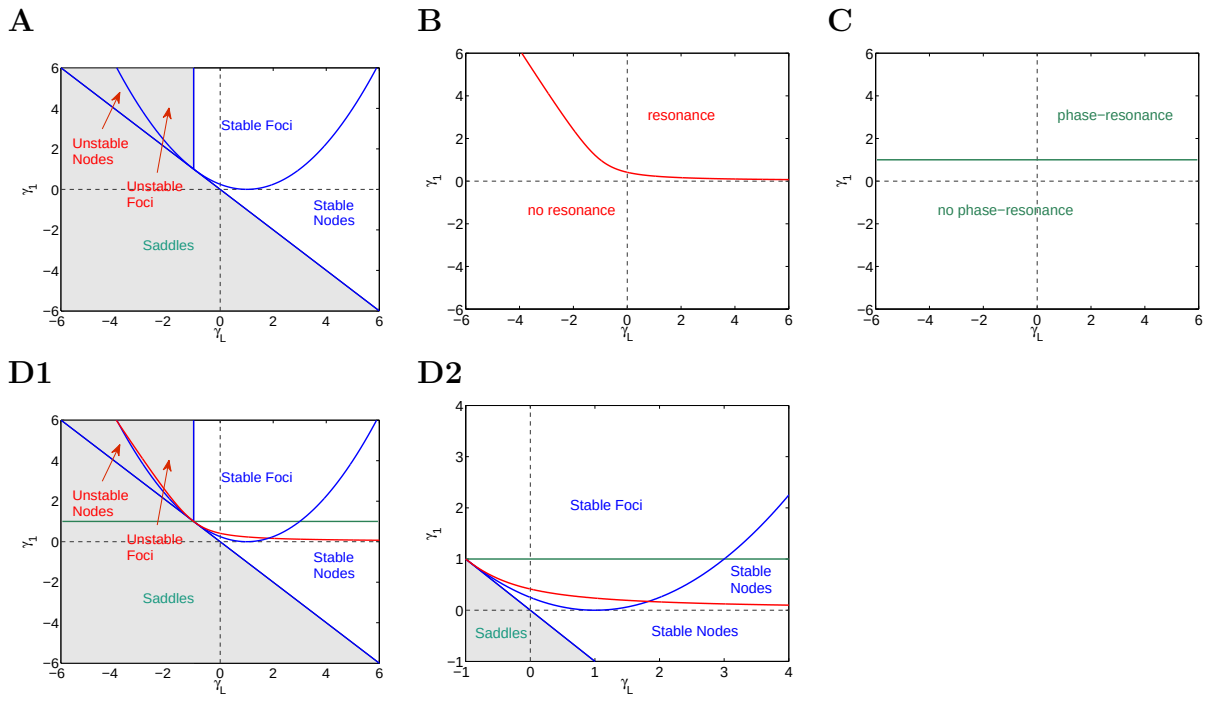

Figure 2: **Stability and resonance diagrams for the reduced 2D linear system (12)-(13) ($\gamma_2 = 0$) in γ_L-γ_1 parameter space.**